NASA TECHNICAL MEMORANDUM

NASA TM X-71889

NASA TM X-71889

(NASA-TM-X-71889) CORRELATIONS AMONG ULTRASONIC PROPAGATION FACTORS AND FRACTURE TOUGHNESS PROPERTIES OF METALLIC MATERIALS (NASA) 31 p HC $4.00 CSCL 11D

N76-21319

G3/26 Unclas 21546

CORRELATIONS AMONG ULTRASONIC PROPAGATION FACTORS AND FRACTURE TOUGHNESS PROPERTIES OF METALLIC MATERIALS

by Alex Vary
Lewis Research Center
Cleveland, Ohio 44135

TECHNICAL PAPER presented at
Spring Conference of the American Society
for Nondestructive Testing
Los Angeles, California, March 8-11, 1976

CORRELATIONS AMONG ULTRASONIC PROPAGATION FACTORS AND FRACTURE TOUGHNESS PROPERTIES OF METALLIC MATERIALS

by Alex Vary

Lewis Research Center

SUMMARY

Empirical evidence is presented to show the close relation that exists between the ultrasonic attenuation properties and fracture toughness (i.e., catastrophic crack propagation) properties of polycrystalline metallic materials. Experimental evidence was obtained by ultrasonically probing specimens of two maraging steels (a 200 and a 250 grade) and a titanium alloy (Ti-8Mo-8V-2Fe-3Al). These specimens had been treated to have a range of fracture toughness values from 51 to 146 MPa$\sqrt{m}$. The specimens also exhibited a variety of yield strengths and microstructures due to constitutive, cold working, and thermal aging differences.

Relevant data were extracted by a frequency spectrum analysis procedure over the frequency range between 10 and 50 MHz. The effect of microstructural factors on ultrasonic attenuation was evaluated in terms of the slope of the attenuation coefficient versus frequency curve characteristic of each specimen material. It was found that the plane strain fracture toughness and also the yield strength of the materials examined were strongly related to the slope of the attenuation versus frequency curve.

This paper gives an account of the methodology that was used to extract the required ultrasonic attenuation information. Problems associated with the methodology are discussed. Both theoretical speculations and tentative experimental data are presented to indicate that plane strain fracture toughness and yield strength can be properly correlated through appropriate ultrasonic propagation factors.

E-8671

SYMBOLS

Units used in the text are indicated when applicable. Fundamental SI dimensions appear in parentheses.

A absorption factor (sm^{-1})

a ultrasonic factor, $= \beta_{\alpha 1} - bK_{Ic}$, $\mu s/cm$ (sm^{-1})

a' constant, = 1, eq. (13)

B	ratio of echo amplitudes relative to frequency
B1,B2	ultrasonic echo amplitude relative to frequency
b	constant, = 10^{-3} μs/(cm MPa $\sqrt{m}$), (N^{-1} s $m^{1/2}$)
b'	constant, eq. (13), $1/\sqrt{m}$, ($m^{-1/2}$)
c	proportionality constant, eq. (7)
c'	constant, eq. (13), (MPa)(cm)/μs, (N s^{-1} m^{-1})
D	average grain diameter, (m)
d'	constant, eq. (13), MPa, (N m^{-2})
E	Young's (elastic) modulus, (N m^{-2})
E'	extensional (elastic) modulus, (N m^{-2})
f	frequency, MHz, (s^{-1})
G_c	critical "energy release factor," eq. (1), (N m^{-1})
K_c	critical stress intensity, MPa$\sqrt{m}$, (N $m^{-3/2}$)
K_{Ic}	plane strain fracture toughness, MPa$\sqrt{m}$, (N $m^{-3/2}$)
K_Q	conditional value of K_{Ic}, MPa$\sqrt{m}$, (N $m^{-3/2}$)
m	exponent, eq. (7)
n	numerical factor
R	reflection coefficient
R_c	Rockwell-C hardness
S_1	scattering factor, (s^4 m^{-4})
S_2	scattering factor, (s^2 m^{-2})
t	specimen thickness, cm, (m)
v_ℓ	longitudinal velocity, cm/μs, (m s^{-1})
Z	acoustic impedance of solid, = ρv, (kg m^{-2} s^{-1})
Z_c	acoustic impedance of couplant, (kg m^{-2} s^{-1})

α attenuation coefficient, Np/cm, (m^{-1})

α_a absorption attenuation coefficient, (m^{-1})

α_s scatter attenuation coefficient, (m^{-1})

β attenuation slope, = $d\alpha/df$, (s m^{-1})

β_δ attenuation slope at $f = v/\lambda$, μs/cm, (s m^{-1})

$\beta_{\alpha 1}$ attenuation slope at $\alpha = 1$, μs/cm, (s m^{-1})

δ (grain) boundary spacing, μm, (m)

λ wavelength, (m)

ν Poisson's ratio

ρ density, g/cm^3, (kg m^{-3})

σ_Y yield strength, MPa, (N m^{-2})

INTRODUCTION

The study described herein was made because there are strong incentives for developing nondestructive ultrasonic methods for evaluating material fracture properties. First, less expensive alternatives would be available to complement and corroborate mechanical destructive tests. Second, nondestructive techniques would be available for use on raw materials or actual hardware to assess or verify mechanical properties. Third, from the standpoint of materials science, continued work of this type should contribute to identification and analysis of factors that control toughness and thus aid in fracture control technology.

This work is a continuation of that described in reference 1. The previous work was a preliminary effort to establish the feasibility of using ultrasonic attenuation measurements to rank metals according to their relative fracture toughness values. The purpose of the present paper is threefold. First, to describe the details and problems associated with the acquisition and processing of ultrasonic data needed to evaluate attenuation characteristics. Second, to show that the resultant attenuation measurements successfully correlate ultrasonic and crack propagation properties of materials. Third, to indicate some tentative theoretical grounds for the empirically observed relations between ultrasonic and crack propagation factors.

The previously mentioned material is presented to encourage further studies of the possible relations involved. Reasons for expecting ultra-

sonic measurements to correlate with fracture toughness properties are given in a background discussion. Relevant prior work is cited therein. Next, the approach and experimental procedures are explained. Finally, the results of this study are presented and discussed. Emphasis is placed on the somewhat tentative nature of these results.

BACKGROUND

Fracture toughness is an intrinsic property that characterizes the fracture behavior of a material. It corresponds to a stress intensity which when a particular size crack is present will cause the crack to propagate catastrophically. Fracture toughness is expressed as a critical stress intensity K_c. It is related to the tensile modulus and critical "strain energy release" factor G_c (refs. 2 and 3).

$$K_c = \sqrt{E' G_c} \tag{1}$$

where E' equals E (Young's modulus) for plane stress and $E/(1 - \nu^2)$ for plane strain conditions. The quantity G_c corresponds to the material's surface tension. It is a measure of the force required to extend a crack's perimeter by a unit length. This quantity has been related to yield strength σ_Y (ref. 3).

$$G_c = n\sigma_Y \delta_c \tag{2}$$

where δ_c is a critical crack opening displacement and n is a numerical coefficient. The coefficient n incorporates strain and associated factors.

From the standpoint of ultrasonic assessment of K_c it is significant that E' in equation (1) is related to ultrasonic velocity v (ref. 4). It is known that K_c is related to a material's microstructure. Because the attenuation of ultrasonic waves (e.g., elastic waves) is likewise related to microstructure, it follows that K_c is related to ultrasonic attenuation properties. Therefore, one should expect a correlation between fracture toughness and ultrasonic propagation properties via ultrasonic velocity and attenuation factors.

Acoustic emission studies have shown that ultrasonic stress waves in metals are emitted by various disturbances; e.g., dislocation motions, microcracking, etc. (refs. 5 and 6). Moreover, acoustic emission studies appear to support the expectation that in high toughness materials the propagation and interaction of these ultrasonic stress waves are inhibited by the attenuation properties of the material (ref. 7). Therefore, during rapid crack growth, the wave propagation properties of the material are probably significant. Ultrasonic attenuation measurements might then be expected to gauge factors that influence crack propagation

and hence fracture toughness.

Some experimental support for the above-stated premise is available. By using shock stressing techniques, it can be shown that sustained crack growth occurs at times corresponding to the presence of a stress wave front at the crack tip. It appears that terminal crack speed is bounded by the stress wave's propagation velocity. Since crack speeds are less than wave velocities, stress wave reflections interact with and influence the growth of a running crack (ref. 8). Various investigators have studied the interaction and influence of ultrasonic waves on crack propagation. For example, it has been shown that imposition of ultrasonic waves will deflect a running crack in a predictable manner (ref. 9). Other studies have shown a close correspondence of brittle fracture and stress waves (refs. 10 and 11). It seems appropriate, therefore, to conduct ultrasonic studies with a particular emphasis on what they can reveal about interactions of spontaneous stress waves during fracture.

APPROACH

Among the causes of ultrasonic attenuation in polycrystalline aggregates is scattering by the microstructure and absorption due to dislocation dampening and elastic hysteresis. Ultrasonic attenuation can be summarized in terms of the attenuation coefficient α, the average grain diameter D, frequency f, and wavelength λ (refs. 4 and 12). The total attenuation coefficient is the sum of the absorption attenuation coefficient, α_a, and the scattering attenuation coefficient α_s:

$$\alpha = \alpha_a + \alpha_s \tag{3}$$

for $\lambda > D$ (Rayleigh scattering domain),

$$\alpha_s = S_1 D^3 f^4 \tag{4}$$

and, for $\lambda \leq D$ (stochastic scattering domain),

$$\alpha_s = S_2 D f^2 \tag{5}$$

and for the absorption domain,

$$\alpha_a = Af \tag{6}$$

where S and A are scattering and absorption factors, respectively. (The factor A may itself be a function of f over a sufficiently great frequency range.)

For heterogeneous engineering materials, the α versus f dependence within a given frequency domain will involve some mixture of the exponents given in the previous equations. It should, therefore, be expected that microstructural variations will produce corresponding variations in the slope of the α versus f curve (refs. 2 and 13). Accordingly, a general form of the attenuation versus frequency relation will be taken as,

$$\alpha = cf^m \tag{7}$$

for the purposes of this study. Since the attenuation measurements in this study were made within a limited frequency regime where equation (7) is applicable, m and c can be considered constants for a given material.

According to reference 1, a material's fracture toughness will vary directly with β the slope of the attenuation versus frequency curve that is characteristic of the material, where $\beta = d\alpha/df$ evaluated at a particular frequency. To find β, therefore, it is necessary to experimentally determine the equation relating α to f for each specimen material.

The procedure used in this study was to ultrasonically probe a series of specimens of materials for which fracture toughness values had been measured. These measurements are conventionally made under conditions that give plane strain fracture toughness values K_{Ic} (ref. 14). The validity of fracture toughness measurements depend on the use of appropriate test and specimen parameters. These vary with the material being tested to ensure that plane strain conditions prevail. The quantity K_{Ic} thus implies a particular K_c value. The approach adopted herein is to examine empirical correlations between K_{Ic} and β, where β is evaluated at appropriate frequencies.

EXPERIMENTAL PROCEDURE

Specimen materials. - The materials used in this study were specimens of three different materials for which fracture toughness values were previously measured. There were five 200-grade maraging steel specimens each aged at a different temperature to obtain a range of fracture toughness and yield strength values. A second set consisted of four specimens with a 250-grade maraging steel composition. This second set was selected because the specimens spanned a wide difference in K_{Ic} values while having virtually identical yield strengths. A third set of four specimens consisted of a titanium alloy with the composition Ti-8Mo-8V-2Fe-3Al. Each of these specimens was aged to have a different toughness and yield strength value.

Pertinent data on the three sets of specimens are given in table I.

The data include plane strain fracture toughness, yield strength, and Rockwell-C hardness values. The values of K_{Ic} cover the range from 51 to 146 MPa$\sqrt{m}$ while the yield strengths vary from 1075 to 1430 MPa.

Fracture toughness measurements quoted herein were made by personnel from the Lewis Research Center Fracture Branch, in conformance with plane strain criteria defined in ASTM E 399-70T, 4.2 (ref. 14). For two specimens, the conditional value K_Q defined in ASTM E 399-70T, 8.1 (ref. 14) is given in place of K_{Ic} in table I. For these two specimens, only the conditional values were available. It can be assumed that the K_Q values are close to the actual K_{Ic} values but that they rank lower in validity. In all cases yield strengths (at 0.2 percent elongation) were obtained by testing duplicates of the fracture toughness specimens. The Rockwell-C hardness values quoted in table I were taken directly from the ultrasonic specimens described in the next section.

Ultrasonic specimens. - The original fracture toughness specimens were sectioned, and a representative rectangular segment was cut from each and ground to size. These segments were used as the ultrasonic test specimens. This procedure ensured that the attenuation properties measured were related specifically to objects that were actually subjects of previous fracture toughness tests. As indicated in figure 1, the ultrasonic specimens were cut from near the fracture surface to further ensure that they were representative.

A small segment of each ultrasonic specimen was reserved for metallographic examination. These were mounted and treated to exhibit their microstructures, as shown in figure 2. The ultrasonic specimens had smooth ground surfaces (32 rms, approximately). The dimensions varied according to the material and the size of the original fracture toughness specimens from which they were sectioned. The thicknesses ranged from 0.25 to 0.30 cm. The thicknesses were selected for compatibility with the ultrasonic probe configuration and signal processing requirements.

The specimen thicknesses varied according to the material so that the time interval between successive echoes was approximately 2 microseconds. This corresponds to roughly one-third the delay time introduced by the fused quartz buffer attached to the transducer crystal (see fig. 3). Thus, at least three echo pulses from the specimen could be acquired within the quartz delay line interval. This afforded a convenient means of getting a clear set of strong signals for subsequent analysis.

Apparatus and procedure. - Ultrasonic velocity and attenuation measurements were made on the previously described ultrasonic specimens. In making these measurements, the ultrasound was directed into the specimens along an axis parallel to the fracture surface of the original fracture toughness specimen. Thus, relative to the microstructure, the ultrasound propagated in the same direction as the crack did in the original K_{Ic} test (see fig. 1).

The apparatus that was used is indicated in figures 3 to 5. The ultrasonic measurements were made using piezoelectric crystal transducers. A cylindrical fused quartz buffer (delay line) was bonded to the transducer crystal. Four broadband piezoelectric transducers were used. Each covered a separate nominal frequency. The transducer nominal (center) frequencies were 10, 20, 30, and 50 MHz. Being broadband the transducer frequencies overlapped to cover the range from less than 10 to greater than 50 MHz. Glycerin was used as the couplant between the quartz buffer and the specimens.

The longitudinal ultrasonic velocity was measured for each specimen through the thickness. Velocity measurements were made at two center frequencies - 10 and 30 MHz. Each specimen was also micrometrically measured and weighed to determine density. From these measurements the acoustic impedance Z was determined and used to calculate the reflection coefficient R for each specimen (ref. 15).

$$R = (Z - Z_c)/(Z + Z_c) \tag{8}$$

The value for R thus obtained was used in a formula for calculating the attenuation coefficient α.

The above-mentioned velocity measurements were made by the "pulse-echo overlap" method (ref. 16). Because of the small specimen thicknesses, a modified version of the method was used. This version involved three rather than the customary two, successive echoes. The first and second echoes were encompassed in one gate while the second and third were encompassed in a second gate as indicated in figure 4. The control oscillator frequency was then adjusted to bring all three echoes into coincidence (overlap). The period corresponding to the oscillator frequency is a measure of the time interval needed for sound to traverse twice the specimen thickness t.

The formula used to calculate the attenuation coefficient α is based on the frequency spectrum analysis method for measuring attenuation. This method is described in references 16 and 17. For the present case, the procedure was restricted to differential spectral analysis of only the first two echoes (B1 and B2) from the back (free) surface of the specimens (see fig. 5). The method of spectrum analysis can also be used to determine R by means of the front surface (FS) echo. Because R was accurately determined separately (by eq. (8)), it was unnecessary to include spectral analysis of the FS echo other than as a check. The amplitude ratio of the echoes $B = (B2/B1)$ was determined for a set of frequencies over the range between 10 and 50 MHz. These values for B were used with the measured values of R to compute α from (ref. 17)

$$\alpha = \ell n(R/B)/2t \tag{9}$$

where t is the specimen thickness. The object of the differential spec-

trum analysis is to generate a set of values of α versus f over a sufficiently wide frequency range (in this case the range between 10 and 50 MHz).

EXPERIMENTAL RESULTS

Reflection coefficient. - The measured ultrasonic propagation velocities and material densities for the thirteen specimens are listed in table II. The longitudinal velocity was measured for each specimen at two frequencies, 10 and 30 MHz. In all instances the 30 MHz velocity exceeds the 10 MHz velocity. However, the difference is slight. It is of the order of 1 percent. This difference is ignorable in calculating the reflection coefficient R from equation (8). Even somewhat larger variations in velocity would have virtually no effect on the value of R in the present case. Therefore, R can be considered constant for the frequency regime involved.

Amplitude ratio characteristic. - A curve typical of the amplitude ratio characteristic (ARC) of the thirteen ultrasonic specimens is presented in figure 6. The ARC curve is a smooth curve based on a set of raw B values that were determined for each of a set of frequencies in the range between 10 and 50 MHz. The determination of the smooth ARC curve is an important first step in the procedure for evaluating the attenuation coefficient α. The ARC curve constitutes the data from which α is calculated for each frequency and is critical in determining the slope of the α versus f curve. There is no established theoretical form for the ARC curve (ref. 12); therefore, this curve was determined empirically by a graphical method as described hereinafter.

As is indicated in figure 6 the value of the reflection coefficient R is an upper bound on the ARC curve. The ARC can neither exceed nor equal R, otherwise negative or zero attenuation coefficients would arise. Clearly, α must be a positive number.

Each data point in figure 6 represents the mean of several (usually 10) raw B values. Generally, frequencies greater than 30 MHz yielded fewer valid values because of low signal-to-noise ratios (at the tail end of the frequency spectra, see fig. 5(b)). The mean B values are bracketed with error bars that represent the scatter in raw B values.

The scatter in raw data arose because of two factors. First, because of the "noisiness" of the microstructures involved. This was ascribable to micro-defects, grain size and shape variations, and similar factors. Second, because the amplitude ratios were obtained by repeating measurements at various probe positions over the specimen. No two probe positions yielded exactly the same raw B value at a given frequency. Indeed, any particular set of B versus f values would tend to characterize local microstructural anomalies as well as the basic (smooth) microstructural properties. This poses a problem in attempting to get a smooth monotonic curve that represents the overall ARC.

The procedure used to circumvent the above problem was to make a sufficient number of measurements. Thus, raw B measurements were made until the mean values that were accumulated for a set of frequencies appeared adequate to construct an ARC curve. This procedure furnished a set of mean B values such as those represented in figure 6. Each mean B value thus obtained is, of course, in error to some degree. The faired ARC curve constitutes a graphical estimation of the probable coordinates of the true mean B values. This approach is recommended until computerized signal averaging methods can be developed to amass the large amounts of data needed to firmly establish the true B versus f (ARC) curve.

Attenuation versus frequency curves. - Values for B were read from the ARC curves and substituted in equation (9) to compute values for the attenuation coefficient α for each of a series of frequencies between 10 and 50 MHz. A logarithmic plot of α versus f was made for each specimen in the above-described manner.

It was found that each of the logarithmic plots tended to linearity and exhibited essentially fixed slopes above approximately 15 MHz. For the frequencies below about 15 MHz the plots deviated from linearity because of geometric diffraction effects. However, only the linear portions of the α versus f plots are of interest. Therefore, a linearized curve based on frequencies of 15 MHz or greater was drawn for each specimen. An example of this is given in figure 7(a). Figure 7(a) also indicates the magnitude of the diffraction error at the low frequencies. This was confirmed by calculating diffraction correction factors for a set of frequencies from 10 to 20 MHz in accordance with reference 18.

Using a linear-regression least-squares method, an equation was determined for the line that best represented the logarithmic α versus f curve of each ultrasonic specimen. This provided a set of values for c and m in equation (7). These parameters, c and m, are given in table II for each specimen.

Figures 7(b) through (d) show the attenuation versus frequency characteristic (AFC) curves for each of the specimens. Each material is grouped according to type: 200-grade maraging steel in figure 7(b), 250-grade maraging steel in figure 7(c), and titanium alloy in figure 7(d). These AFC curves are based on the c and m parameter values listed in table II.

The parameters c and m are taken herein to hold for all frequencies from 10 to over 50 MHz. This assumption is deemed appropriate as a first approximation for the purpose of evaluating β at the higher frequencies. It is probable that the actual α versus f curve deviates from linearity in the higher frequency region due to wavelength-to-grain size ratio variations (see eq. (4) to (6)). Thus, the linear AFC curve parameters, c and m, probably tend to give β values that are too

great at the extreme frequencies. However, the experimental method used did not permit determining the exact relation of α to f at frequencies greater than approximately 50 MHz. Herein, it is simply assumed that the linear AFC curve can be meaningfully extrapolated to about 640 MHz. This latter frequency is associated with wavelengths determined in accordance with the grain boundary spacing dimension described next.

Metallography. - Figure 2 shows typical microstructures of each of the specimens. These photomicrographs were used for estimating the average spacing of grain boundaries. The grain structure of the titanium alloy is readily apparent, e.g., figure 2(h). Thus, the grain boundary spacing of this material is easily measurable. For the 200-grade maraging steel specimens it is quite difficult to identify a grain structure, e.g., figure 2(a). However, it is possible to discern groups of parallel linear features in these specimens (i.e., twinning or subgrain boundaries). Since these features probably affect the transmission of ultrasonic waves in the same manner as grain boundaries, they were used to determine an average "grain boundary" spacing for the maraging steels. Herein, an average (grain) boundary spacing was taken as characteristic of each specimen. This average spacing dimension δ was determined in accordance with the ASTM intercept procedure described in reference 19. Measurements were taken from both 100X and 250X photomicrographs such as those depicted in figure 2.

As explained hereinafter, the above-described estimate of (grain) boundary spacing δ will determine a particular wavelength λ (i.e., λ will be set equal to δ). This wavelength λ determines the frequency used in evaluating β. The spacing dimension δ for each specimen is indicated in table II.

ANALYSIS OF RESULTS

Method of analysis. - The principal ultrasonic quantity used herein to correlate ultrasonic with fracture toughness properties is β the slope of the AFC curve. The quantity β was evaluated in two ways: (a) relative to a "standard" attenuation, and (b) relative to a "critical" wavelength:

(a) First, noting that $\beta = d\alpha/df$ and given equation (7) we have

$$\beta = cmf^{m-1} = \alpha m/f \tag{10}$$

Letting $\beta_{\alpha 1}$ be the value of β evaluated at the frequency where $\alpha = 1$, i.e., at unit ("standard") attenuation, then

$$\beta_{\alpha 1} = mc^{1/m} \tag{11}$$

(b) The second method of evaluating β involves the selection of a particular frequency for substitution in equation (10). This particular value for f is taken as that associated with a "critical" or resonance wavelength, here taken equal to the (grain) boundary spacing dimension δ. The corresponding value of β is labeled β_δ.

Analysis of the results of this study indicated that the product $v_\ell \beta_\delta$ correlates strongly with the quantity K_{Ic}^2/σ_Y. It was also found that the quantity $\beta_{\alpha 1}$ correlates strongly with K_{Ic}. The values for $\beta_{\alpha 1}$, β_δ, and $v_\ell \beta_\delta$ were determined for each specimen and are listed in table II.

The $\beta_{\alpha 1}$ factor. - Figure 8 is a plot of $\beta_{\alpha 1}$ versus K_{Ic} for all the specimens. Inspection of figure 8 shows that the data can be grouped according to yield strength. For example, the four data points for the 250-grade maraging steel specimens fall on the same line. These four specimens have virtually identical yield strengths. Also, two pairs of 200 grade maraging steel and one pair of titanium alloy specimens had like yield strengths (within 10 MPa). These data pairs can be connected with straight lines that parallel that for the 250 grade maraging steel. The pattern that emerges is indicated by the sets of parallel lines drawn through the data for the various specimen materials. Each line is labeled with the (approximate) yield strength shared by the data points it includes. The $\beta_{\alpha 1}$ versus K_{Ic} plot for each material (fig. 8) thus appears to consist of a set of lines that are isometric with respect to σ_Y.

$$\beta_{\alpha 1} = a + bK_{Ic} \tag{12}$$

where a is a function of σ_Y and b is a conversion factor equal to 1×10^{-3} $\mu s/(cmMPa\sqrt{m})$. (Note that the lines in fig. 8 all apparently share a common slope of unity.)

The information in figure 8 can be developed further. Assuming that the above linear isometric grouping is correct, an equation can be determined for each line. This gives a set of values for a in equation (12) for specimens sharing the same yield strength, where $a = \beta_{\alpha 1} - bK_{Ic}$. Accordingly, figure 9(a) is a plot of yield strength σ_Y versus a (herein termed the "ultrasonic factor") for the two materials for which there are sufficient data to make this plot: the 200-grade maraging steel and the titanium alloy. It is apparent from this plot that the data for these two materials produce linear correlations between yield strength and the ultrasonic factor a.

It is instructive to compare figure 9(a) with figure 9(b) which is a conventional plot of yield strength versus fracture toughness σ_Y versus K_{Ic} for these two materials. This plot indicates the general trend of decreasing yield strength with increasing fracture toughness. Also apparent is the considerable deviation from this general trend. Comparison of the two figures, 9(a) and (b), indicates that ultrasonic factors can be used to better establish the relation between σ_Y and K_{Ic}.

Obviously, introduction of the ultrasonic factor a brings more coherence to the relation between K_{Ic} and σ_Y. Figure 9(a) thus suggests the following general relation.

$$a'\sigma_Y + b'K_{Ic} + c'\beta_{\alpha 1} = d' \tag{13}$$

where, based on figure 9(a), the equation for the 200-grade maraging steel is

$$\sigma_Y + 17K_{Ic} - 17\times10^3\ \beta_{\alpha 1} = 1490 \tag{13a}$$

and the equation for the titanium alloy is

$$\sigma_Y - 8.1K_{Ic} + 8.1\times10^3\ \beta_{\alpha 1} = 1190 \tag{13b}$$

It should be noted that $\beta_{\alpha 1}$ was evaluated at frequencies where the AFC curve was most valid; i.e., required either little or no extrapolation.

The $v_\ell\beta_\delta$ factor. - Figure 10 is a plot of $v_\ell\beta_\delta$ versus K_{Ic}^2/σ_Y for all the specimens tested. A linear regression curve fit was made for the data shown in figure 10. The goodness-of-fit is 0.99 for the curve of figure 10. This curve has the equation

$$v_\ell\beta_\delta = 8.07\times10^{-21}(K_{Ic}^2/\sigma_Y)^{2.91} \tag{14}$$

or, by solving for K_{Ic}^2/σ_Y,

$$K_{Ic}^2/\sigma_Y = 8.12\times10^6(v_\ell\beta_\delta)^{0.344} \tag{15}$$

Thus the quantity K_{Ic}^2/σ_Y apparently varies nearly as the cube root of $v_\ell\beta_\delta$. However, the AFC curves probably give too high values for β_δ (as was mentioned previously relative to fig. 7). Therefore, the actual exponent on $v_\ell\beta_\delta$ in equation (15) is probably greater than that which is indicated by the current data.

DISCUSSION

Interpretations. - The foregoing relations illustrate that fracture toughness, yield strength and, by implication, associated material properties, are intimately connected with ultrasonic propagation properties. It appears, for example, that K_{Ic} and σ_Y can be properly correlated with each other via material factors such as those related to the quantity $\beta_{\alpha 1}$, see figure 9(a).

A possible theoretical basis for the observed relations can be deduced from the concepts introduced in the BACKGROUND section of this report. Briefly, one can postulate that the physical processes involved in crack propagation depend on the propagation and interactions of stress waves.

It might be noted that there is nothing extraordinary in the proposition that stress or sound waves promote cracking ahead of the crack front. One need only recall that concentrated sound of the proper pitch can shatter a highly stressed solid (e.g., a crystal goblet). Moreover, the process need not involve contiguous regions. It probably involves microfractures and crack nucleations at a distance from the main crack front. In this context, it seems that the previously stated premise and empirical results prove to be complementary.

An alternative explanation of the empirical correlations can be based on ultrasonic attenuation as a measure of the distribution density of subgranular scattering centers or dislocations. Ultimately, K_c, σ_Y, and β are, of course, determined by the number and mobility of dislocations (refs. 3 and 6). Therefore, it can be argued that the empirical correlations testify that the ultrasonic factors $\beta_{\alpha 1}$ and β_δ simply measure dislocation densities or loop lengths. In this case absorption attenuation would tend to predominate, and the α versus f curves in figures 7(b) through (e) should all have slopes near unity, according to equation (6). The data in table II show that the α versus f slopes (the m values) are predominantly 2 or greater (at least in the frequency domain of the actual measurements). It is probable that some mixture of absorption and Rayleigh and stochastic scattering was involved within the frequency domain where α was determined. Regardless of the exact mode of ultrasonic wave energy dissipation, I believe that the results herein suggest that the factors $\beta_{\alpha 1}$ and $v_\ell \beta_\delta$ are indirect measures of stress wave energy losses during crack growth.

With reference to figure 10, both the quantities $v_\ell \beta_\delta$ and K_{Ic}^2/σ_Y are related to energy. The latter has the dimensions of specific energy (i.e., energy per unit area). If the dimensionless quantity $v_\ell \beta_\delta$ is a measure of energy loss by stress wave attenuation, it is not surprising that $v_\ell \beta_\delta$ and K_{Ic}^2/σ_Y correlate well irrespective of the materials involved. It is surprising, though, that the strong correlation seen in figure 10 was obtained despite the approximations and extrapolations made in evaluating β_δ. For example, β_δ was somewhat crudely evaluated. To evaluate β_δ it was assumed that the equations for attenuation curves in the frequency range from 10 to 50 MHz applied over the extended frequency domain (up to 640 MHz) associated with crack extension stress waves. This extrapolation was needed to overcome the frequency limitation of the ultrasonic equipment used. It appears, therefore, that ultrasonic probing in this lower frequency domain gives a measure that is proportional to the energy that is potentially transferable to crack extension involving the higher frequency stress waves.

Equation 13, which is based on figures 8 and 9, is interesting from the standpoint of an implied energy partition among the various terms: K_{Ic}, σ_Y, and $\beta_{\alpha 1}$. The terms in equation (13) are probably related to an energy partition among plastic deformation, crack nucleations, and stress wave interactions. Based on the limited results of this study, it appears that the coefficient of K_{Ic} or b' in equation (13) will be positive or negative depending on the mode of fracture. If it is predominantly ductile as in the 200 grade maraging steel (fig. 11(a)), then b' is positive, as in equation (13a). If brittle fracture predominates as in the titanium alloy (fig. 11(b)), then b' is negative, as in equation (13b). The sign of c' is opposite that of b'. Apparently this depends upon whether the crack nucleation sites are energy sources or sinks during fracture.

The data reported thus far is, of course, inadequate to confirm the above speculations. More work is needed to establish the attenuation properties of a wider range of materials for which fracture toughness data can be obtained. In particular, advanced electronic signal processing and computer processing methods will be essential to amass and analyze the ultrasonic signals involved over a considerably greater frequency domain. In situ signal averaging procedures will be needed to reduce the inherent scatter and grain noise effects that attend acquisition of the raw B (amplitude ratio) data.

Applications. - Given empirical relations such as those in equations (13a), (13b), and (14), nondestructive ultrasonic measurements can apparently be used to determine fracture toughness and yield strength values. This could be done by simultaneous solution of pairs of equations, such as equations (13a) and (14), if the quantities $\beta_{\alpha 1}$ and $v_\ell \beta_\delta$ are known. Of course, other data are needed to evaluate the latter quantities. It would be necessary to identify the material and its grain boundary spacing dimension δ. Conceivably, further refinement of ultrasonic methods can produce this additional information (e.g., through relations such as those in eqs. (4) and (5), see ref. 12).

It is reasonable to conclude that once having established appropriate parameters for a material, ultrasonic methods can be used to compile fracture toughness data for subsequent specimens of a given material. This could be accomplished with specimens that are considerably smaller than conventional fracture toughness specimens. These ultrasonic specimens would have to meet certain specifications. As a minimum, they should be dimensioned in accordance with the ultrasonic probe requirements to ensure adequate signal recovery. This type of requirement may pose difficult problems in attempts to adopt the technique to some actual hardware items. However, it is possible to foresee computer-assisted transducers that can adapt the technique to field applications.

Perhaps the most significant implications of the correlations reported herein are concerned with analysis of fracture micromechanics and

hence with fracture control technology. It appears that nondestructive ultrasonic measurements can be an important adjuct to mechanical destructive testing. For example, the interpretation of the relations between K_{Ic} and σ_Y are clarified by the additional data provided by the ultrasonic factors $\beta_{\alpha 1}$ and $v_\ell \beta_\delta$, as in figures 8 to 10.

SUMMARY OF RESULTS

The results presented herein indicate a close relation between rapid crack extension and ultrasonic (stress) wave propagation phenomena in metallic materials (two grades of maraging steel and a titanium alloy). The correlations were obtained by ultrasonically probing specimens of these materials for which fracture toughness and yield strength were previously measured.

Two major empirical relations between ultrasonic and crack (fracture) toughness factors are developed in this report. The first of these involves the plane strain fracture toughness value K_{Ic} and the ultrasonic attenuation factor $\beta_{\alpha 1}$. The quantity $\beta_{\alpha 1}$ is the slope of the attenuation coefficient α versus frequency f curve (i.e., $\beta = d\alpha/df$) evaluated at the frequency where α equals unity. The second correlation involves the specific energy term K_{Ic}^2/σ_Y and the ultrasonic factor $v_\ell \beta_\delta$. The quantity β_δ is the slope of the α versus f curve evaluated at the frequency corresponding to a particular wavelength. This wavelength is determined by a spacing dimension δ that is characteristic of the material's microstructure, i.e., grain boundary spacing. The quantity v_ℓ is longitudinal velocity of the ultrasound and σ_Y is the material's yield strength. Strong correlations were found for $\beta_{\alpha 1}$ versus K_{Ic} and for $v_\ell \beta_\delta$ versus K_{Ic}^2/σ_Y for the four materials studied.

The results indicate that the $v_\ell \beta_\delta$ versus K_{Ic}^2/σ_Y data for all the specimen materials evaluated can be represented by a single curve having the general form.

$$K_{Ic}^2/\sigma_Y = \Psi(v_\ell \beta_\delta)^\theta$$

The relation between $\beta_{\alpha 1}$ and K_{Ic} is more complex since it involves a family of curves that are isometric with respect to σ_Y. For two of the specimen materials sufficient data were available to obtain relations among K_{Ic}, σ_Y, and $\beta_{\alpha 1}$. Thus, for the 200 grade maraging steel and the titanium alloy these relations had the general form

$$a'\sigma_Y + b'K_{Ic} + c'\beta_{\alpha 1} = d'$$

In this latter relation the algebraic signs of b' and c' are opposite and apparently determined by the dominant fracture mode (brittle or ductile).

7. Yosio Nakamura, C. L. Veach, and B. O. McCauley, "Amplitude Distribution of Acoustic Emission Signals," Acoustic Emission, ASTM STP-505, 1972, pp. 164-186, American Society for Testing and Materials, Philadelphia.

8. H. Kolsky and D. Rader, "Stress Waves and Fracture," Fracture - An Advanced Treatise, Ch. 9, Harold Liebowitz, ed., vol. 1, 1971, pp. 533-567, Academic Press, New York.

9. F. Kerkhof, "Wave Fractographic Investigations of Brittle Fracture Dynamics," Proceedings of an International Conference on Dynamic Crack Propagation, George C. Sih, ed., 1973, pp. 3-35, Noordhoff International Publ., Leyden, The Netherlands.

10. H. Kolsky, "Recent Work on the Relations Between Stress Pulses and Fracture," Proceedings of an International Conference on Dynamic Crack Propagation, George C. Sih, ed., 1973, pp. 399-414, Noordhoff International Publ., Leyden, The Netherlands.

11. H. C. vanElst, "The Relation between Increase in Crack Arrest Temperature and Decrease of Stress Wave Attenuation by Material Embrittlement," Proceedings of an International Conference on Dynamic Crack Propagation, George C. Sih, ed., 1973, pp. 283-320, Noordhoff International Publ., Leyden, The Netherlands.

12. Emmanuel P. Papadakis, "Ultrasonic Attenuation Caused by Scattering in Polycrystalline Metals," Journal of the Acoustical Society of America, Vol. 37, Apr. 1965, pp. 711-717.

13. R. L. Roderick and R. Truell, "The Measurement of Ultrasonic Attenuation in Solids by the Pulse of Technique and Some Results in Steel," Journal of Applied Physics, Vol. 23, Feb. 1952, pp. 267-279.

14. W. F. Brown, Jr., ed., Review of Developments in Plane Strain Fracture Toughness Testing, ASTM STP-463, 1970, American Society for Testing and Materials, Philadelphia.

15. J. Krautkramer and H. Krautkramer (B. W. Zenzinger, trans.), Ultrasonic Testing of Materials, 1969, pp. 21-22; 91-100, Springer-Verlag, New York.

16. E. P. Papadakis, "The Measurement of Small Changes in Ultrasonic Velocity and Attenuation," Critical Reviews in Solid State Sciences, Vol. 4, Aug. 1973, pp. 373-418.

17. L. C. Lynnworth, "Attenuation and Reflection Coefficient Nonogram," Ultrasonics, Vol. 12, 1974, pp. 72-73.

18. Emmanuel P. Papadakis, "Ultrasonic Diffraction Loss and Phase Change in Anisotropic Materials," Journal of the Acoustical Society of America, Vol. 40, Oct. 1966, pp. 863-874.

19. 1973 Annual Book of ASTM Standards, Part 31, 1973, p. 422, American Society for Testing and Materials, Philadelphia.

TABLE I. - CHARACTERISTICS OF SPECIMEN MATERIALS

Specimen	Aging temperature, K	Hardness Rockwell, R_c	Yield strength,[d] σ_Y, MPa	Fracture toughness,[e] K_{Ic}, $MPa\sqrt{m}$	Energy parameter, K_{Ic}^2/σ_Y, MJ/m^2
[a]1-200	700	39.9	1320	(113)	9.67
[a]2-200	728	42.9	1430	98.1	6.73
[a]3-200	756	43.2	1430	92.3	5.96
[a]4-200	783	42.8	1330	103	7.98
[a]5-200	811	40.9	1210	(110)	9.98
[b]1-250	672	45.7	1400	118	9.94
[b]2-250	672	45.7	1400	117	9.77
[b]3-250	838	46.1	1400	139	13.8
[b]4-250	838	46.1	1400	146	15.2
[c]1-Ti	700	37.5	1075	53.7	2.68
[c]2-Ti	756	43.4	1370	51.0	1.90
[c]3-Ti	811	41.1	1230	59.9	2.92
[c]4-Ti	867	38.0	1085	70.0	4.52

[a]200 grade maraging steel, cold rolled 50 percent, and aged for 8 hours.

[b]250 grade maraging steel, annealed at 1090 K, air cooled, and aged for 6 hours.

[c]Titanium alloy (Ti-8Mo-8V-2Fe-3Al composition), solution heat treated at 1144 K for 1 hour, water quenched, and aged 8 hours.

[d]Yield strength measured at 0.2 percent elongation (to convert to ksi, divide by 6.89).

[e]Plane strain, conditional K_Q values in parentheses (to convert to $ksi\sqrt{in.}$, divide by 1.10).

TABLE II. - CHARACTERISTICS OF ULTRASONIC SPECIMENS

Specimen	Thickness, t, cm	Density, ρ, g/cm^3	Boundary spacing,[a] δ, μm	Velocity,[b] v_ℓ, $cm/\mu s$	AFC[c] parameters		AFC[d] slope factors		
					c	m	$\beta_{\alpha 1}$, $\mu s/cm$	β_δ, $\mu s/cm$	$v_\ell \beta_\delta$
1-200	0.246	8.03	12.5	0.564	2.22×10^{-3}	2.061	0.106	3.00	1.69
2-200	.246	8.03	12.5	.563	3.46×10^{-3}	1.896	.0955	1.56	.881
3-200	.246	8.03	14.0	.564	5.28×10^{-3}	1.760	.0894	.887	.500
4-200	.246	8.03	14.5	.564	2.02×10^{-3}	2.024	.0944	1.83	1.03
5-200	.246	8.03	13.5	.558	7.75×10^{-4}	2.255	.0941	3.35	1.87
1-250	.248	8.03	8.5	.546	3.81×10^{-5}	2.595	.0514	2.97	1.62
2-250	.249	8.03	8.5	.543	2.62×10^{-5}	2.661	.0505	3.18	1.73
3-250	.248	8.03	13.0	.556	1.41×10^{-5}	2.996	.0720	7.54	4.19
4-250	.246	8.03	13.0	.556	1.56×10^{-5}	3.034	.0790	10.6	5.92
1-Ti	.299	4.75	165	.576	4.38×10^{-2}	1.123	.0692	0.0762	0.0439
2-Ti	.306	4.75	135	.590	3.98×10^{-3}	1.437	.0307	.0298	.0176
3-Ti	.303	4.75	130	.591	2.27×10^{-4}	2.248	.0538	.0597	.0353
4-Ti	.304	4.74	110	.586	5.63×10^{-5}	2.803	.0855	.205	.120

[a]Grain boundary spacing dimension. Frequency used to evaluate β_δ is $f = v/\delta$.

[b]Longitudinal velocity in specimen at center frequency of 30 MHz.

[c]AFC is attenuation coefficient versus frequency characteristic (curve), $\alpha = cf^m$.

[d]$\beta_{\alpha 1} = mc^{1/m}$ and $\beta_\delta = mc(v/\delta)^{m-1}$.

ULTRASONIC SPECIMEN DIMENSIONS:

200 GRADE MARAGING STEEL, d = 1.55 CM, h = 1.95 CM, t = 0.25 CM.
250 GRADE MARAGING STEEL, d = 2.00 CM, h = 2.55 CM, t = 0.25 CM.
TITANIUM ALLOY, d = 2.55 CM, h = 3.15 CM, t = 0.30 CM.

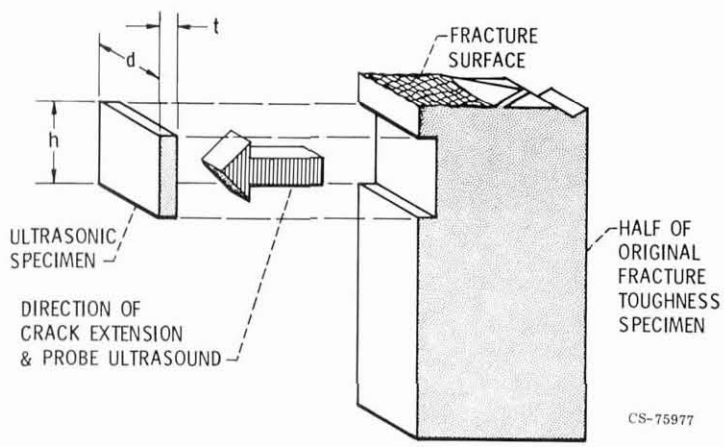

Figure 1. - Typical excision of ultrasonic specimen from fracture toughness specimen.

(a) SPECIMEN 1-200 (200 GRADE MARAGING STEEL).

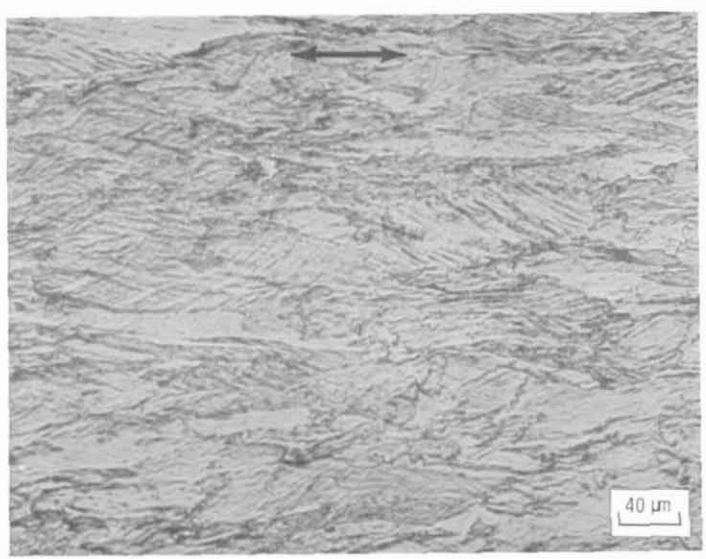

(b) SPECIMEN 2-200 (200 GRADE MARAGING STEEL).

Figure 2. - Photomicrographs of specimen materials. Original magnifications were X100 and X250. Double arrows show direction of probe ultrasound and crack propagation relative to microstructure. Etchant for 200 grade maraging steel was Nital. Etchant for 250 grade maraging steel was Callings. Etchant for titanium alloy was Nitric (+ HF).

(c) SPECIMEN 3-200 (200 GRADE MARAGING STEEL).

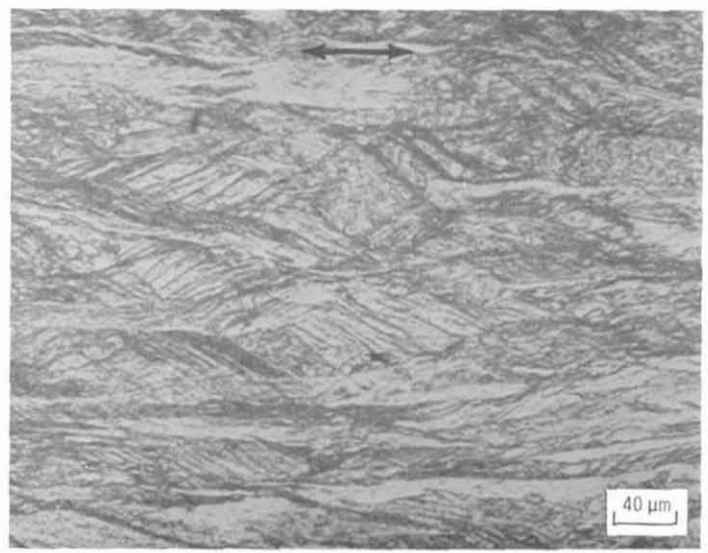

(d) SPECIMEN 5-200 (200 GRADE MARAGING STEEL). SPECIMEN 4-200 IS SIMILAR MICROSTRUCTURALLY.

Figure 2. - Continued.

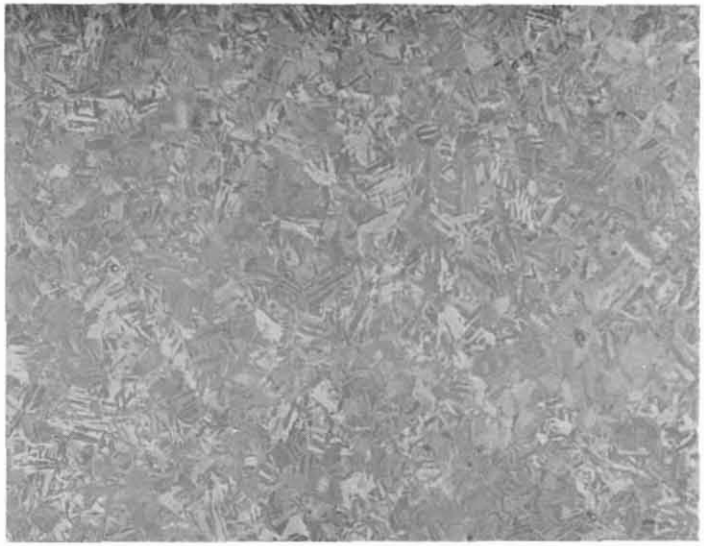

(e) SPECIMEN 1-250 (250 GRADE MARAGING STEEL). SPECIMEN 2-250 IS SIMILAR MICROSTRUCTURALLY.

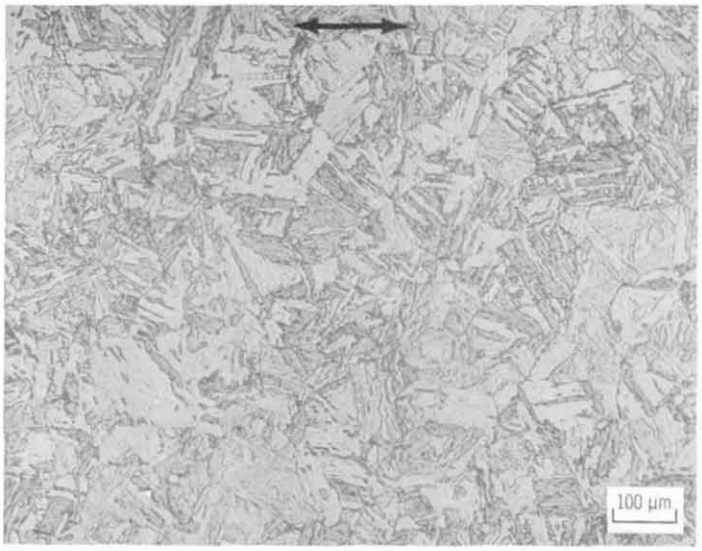

(f) SPECIMEN 3-250 (250 GRADE MARAGING STEEL). SPECIMEN 4-250 IS SIMILAR MICROSTRUCTURALLY.

Figure 2. - Continued.

(g) SPECIMEN 1-Ti (TITANIUM ALLOY).

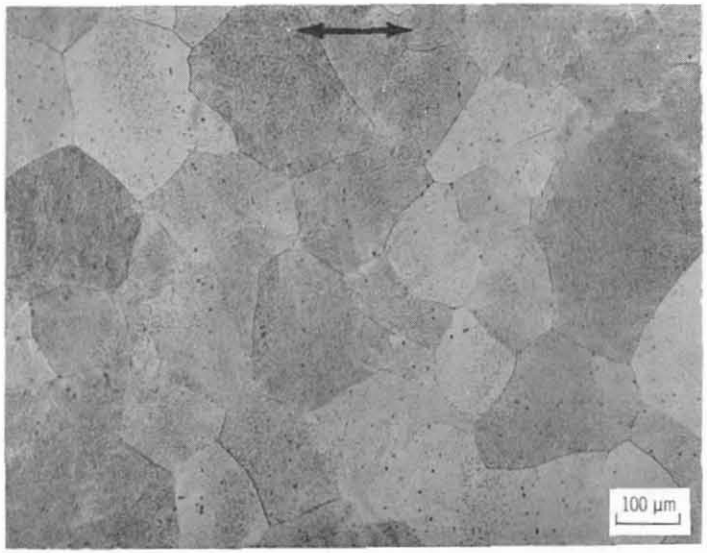

(h) SPECIMEN 4-Ti (TITANIUM ALLOY). SPECIMENS 2-Ti AND 3-Ti ARE SIMILAR MICROSTRUCTURALLY.

Figure 2. - Concluded.

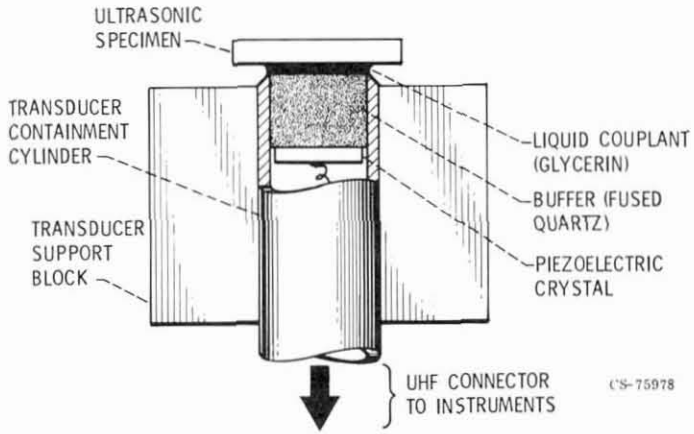

Figure 3. - Configuration of ultrasonic transducer and specimen for making velocity and attenuation measurements.

LEGEND

S IS THE SYNCRONIZATION SIGNAL TO THE OSCILLOSCOPE TIME BASE. THIS SIGNAL IS DERIVED FROM THE OSCILLATOR OUTPUT.

X IS THE SIGNAL TO THE OSCILLOSCOPE HORIZONTAL AMPLIFIER. THE AMPLITUDE OF X DEPENDS ON THE OSCILLATOR FREQUENCY. THIS SIGNAL IS USED TO CONVOLVE THE Y SIGNAL, SEE FIG. 4(b).

Y IS THE SIGNAL TO THE OSCILLOSCOPE VERTICAL AMPLIFIER. THE Y SIGNAL CORRESPONDS TO THE ULTRASONIC ECHOES RECEIVED BY THE TRANSDUCER DURING EACH PULSE INTERVAL.

Z IS THE SIGNAL TO THE OSCILLOSCOPE TRACE INTENSIFIER. THE TRACE INTENSITY IS MADE STRONGER FOR PORTIONS OF THE Y SIGNAL THAT ARE BRACKETED WITHIN GATES Z1 AND Z2.

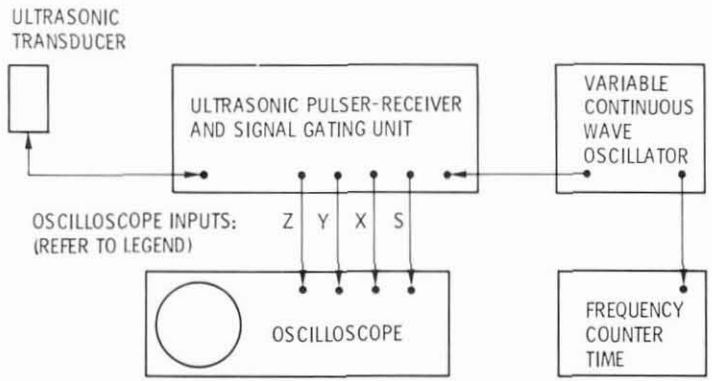

(a) APPARATUS FOR ULTRASONIC VELOCITY MEASUREMENT.

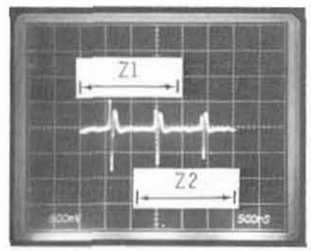

OSCILLOSCOPE TRACE OF Y SIGNAL INDICATING GATES Z1 AND Z2.

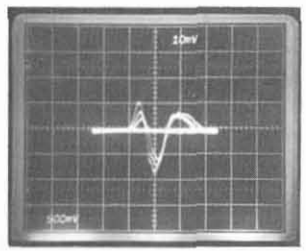

OSCILLOSCOPE TRACE OF CONVOLUTED Y SIGNAL WITH THREE ECHOES OVERLAPPED.

(b) SIGNALS USED IN VELOCITY MEASUREMENT.

Figure 4. - Diagram of apparatus and signal treatment used in ultrasonic velocity measurement by the pulse-echo overlap method.

LEGEND

FS IS THE ECHO RETURNED BY THE SPECIMEN FRONT SURFACE.

B1 IS THE FIRST ECHO FROM THE SPECIMEN BACK (FREE) SURFACE.

B2 IS THE SECOND ECHO FROM THE SPECIMEN BACK (FREE) SURFACE.

ECHOES B1 AND B2 ARE ELECTRONICALLY GATED AND EACH IS SEPARATELY SPECTRUM ANALYZED, SEE FIG. 5(b).

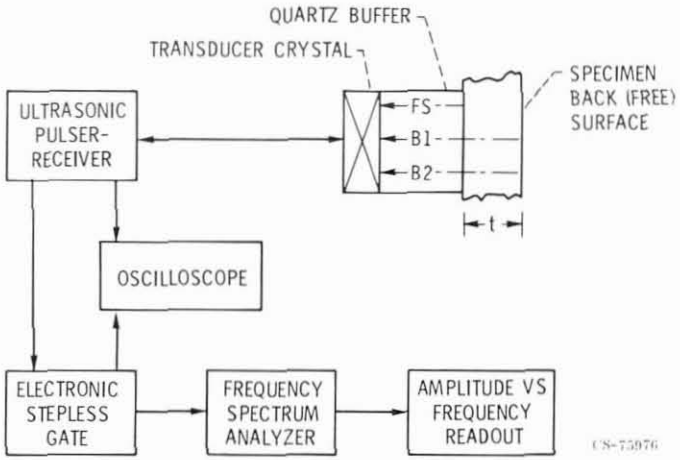

(a) APPARATUS FOR ULTRASONIC ATTENUATION MEASUREMENT.

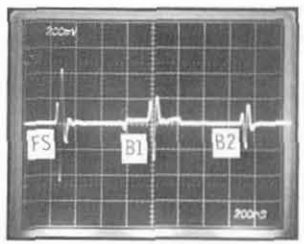

OSCILLOSCOPE TRACE OF FRONT SURFACE (FS) FIRST BACK SURFACE (B1) AND SECOND BACK SURFACE (B2) (TYPICAL) ECHOES.

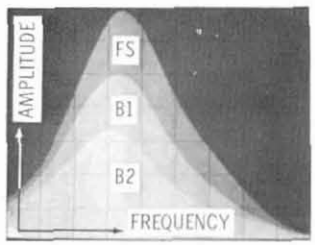

TRIPLE EXPOSURE OF FREQUENCY SPECTRA RELATED TO ECHOES FS, B1, AND B2 (FOR ARBITRARY FREQUENCY AND AMPLITUDE).

(b) SIGNALS AND FREQUENCY SPECTRA USED IN ATTENUATION MEASUREMENTS.

Figure 5. - Diagram of apparatus and signal treatment used in ultrasonic attenuation measurement by the frequency spectrum analysis method.

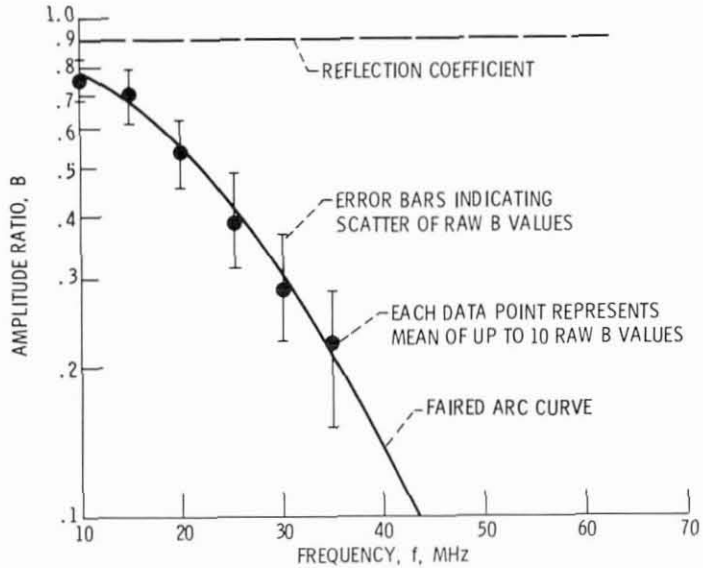

Figure 6. - Typical amplitude ratio characteristic (ARC) curve with explanatory annotation.

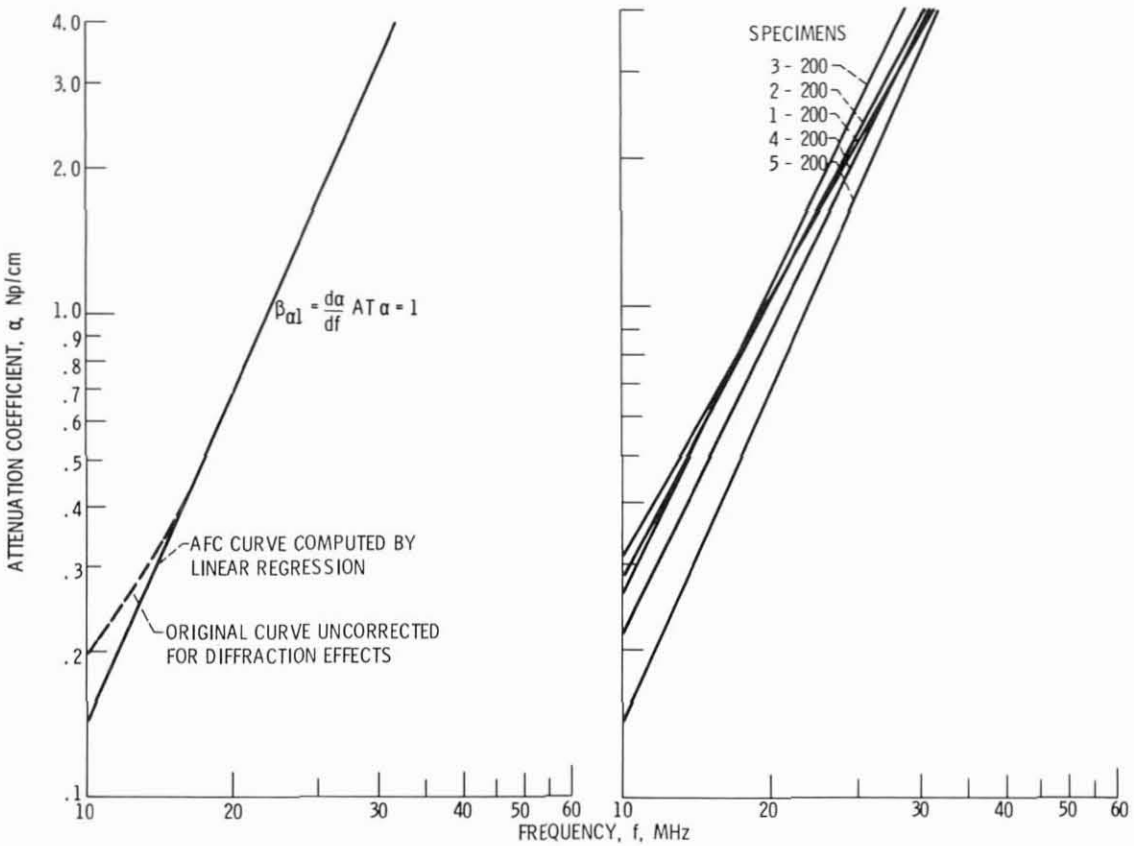

(a) TYPICAL AFC CURVE AND ORIGINAL CURVE (DOTTED) INDICATING MAGNITUDE OF DIFFRACTION EFFECT.

(b) AFC CURVES FOR 200 GRADE MARAGING STEEL SPECIMENS.

Figure 7. - Attenuation coefficient vs. frequency characteristic (AFC) curves.

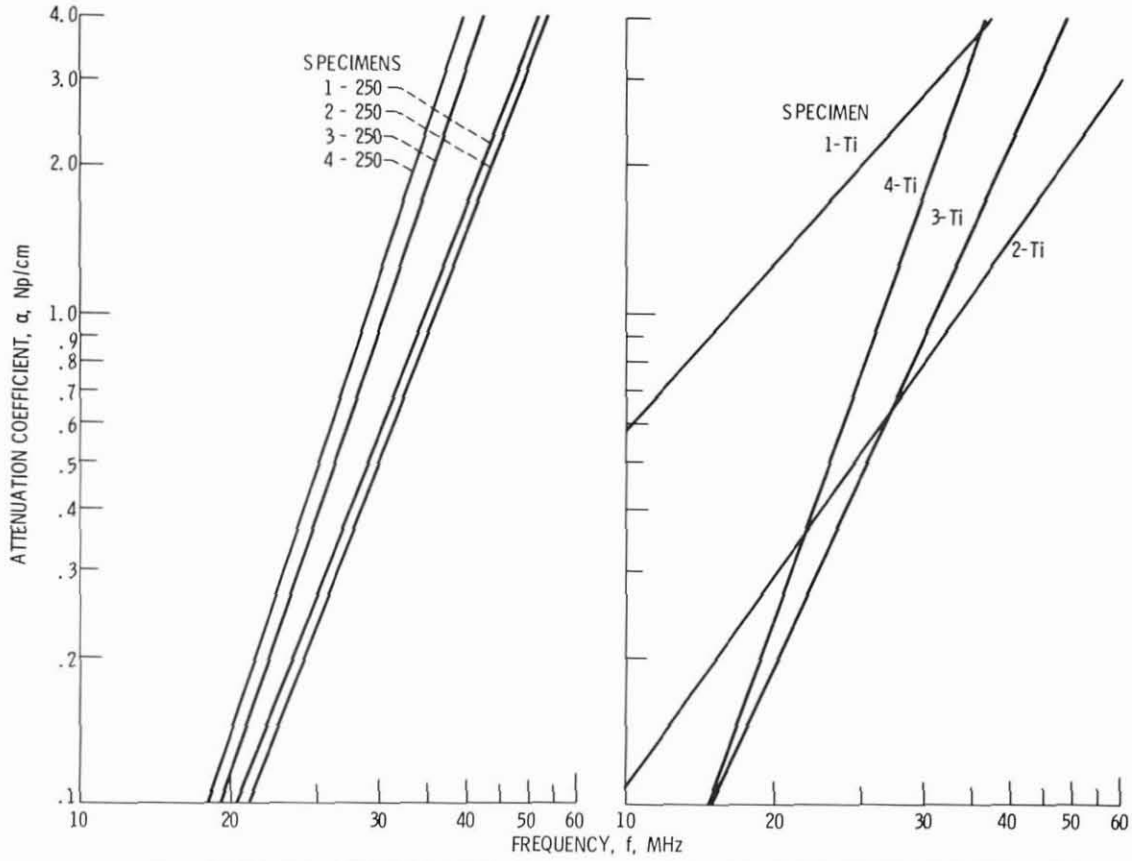

(c) AFC CURVES FOR 250 GRADE MARAGING STEEL SPECIMENS.

(d) AFC CURVES FOR TITANIUM ALLOY SPECIMENS.

Figure 7. - Concluded.

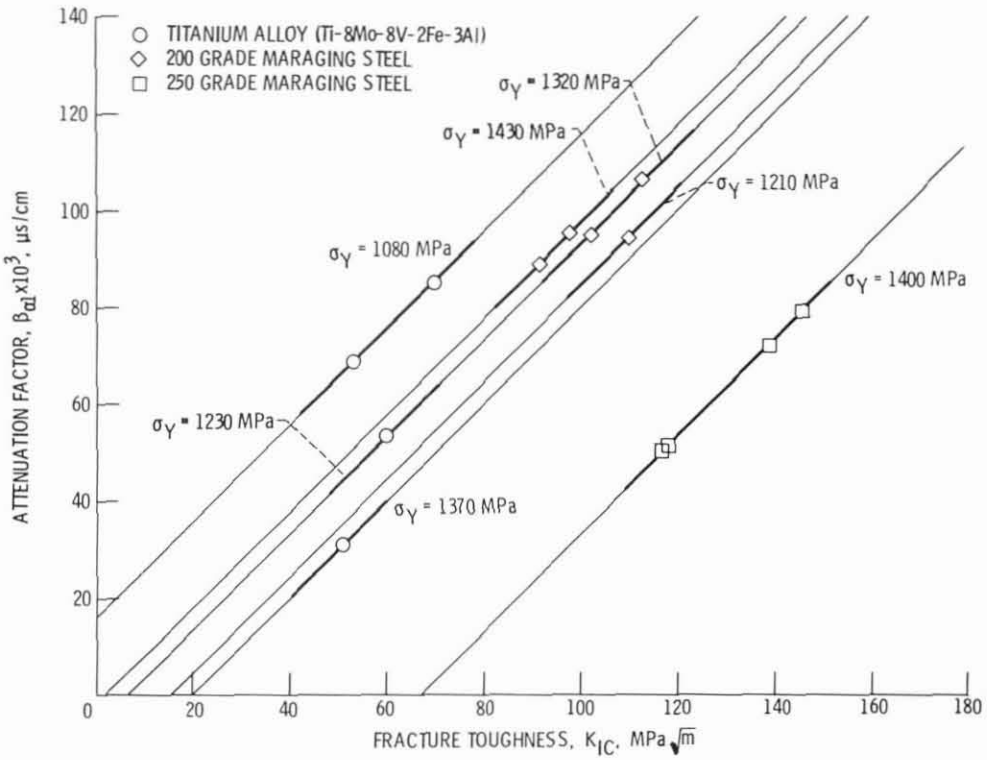

Figure 8. - Ultrasonic attenuation factor $\beta_{\alpha 1}$ as a function of fracture toughness K_{IC} and yield strength σ_Y.

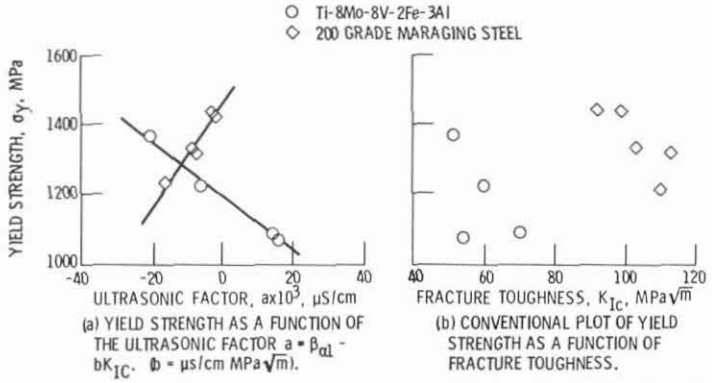

(a) YIELD STRENGTH AS A FUNCTION OF THE ULTRASONIC FACTOR $a = \beta_{\alpha l} - bK_{IC}$. (b = μs/cm MPa$\sqrt{m}$).

(b) CONVENTIONAL PLOT OF YIELD STRENGTH AS A FUNCTION OF FRACTURE TOUGHNESS.

Figure 9. - Correlation of yield strength to fracture toughness for a titanium alloy and a maraging steel.

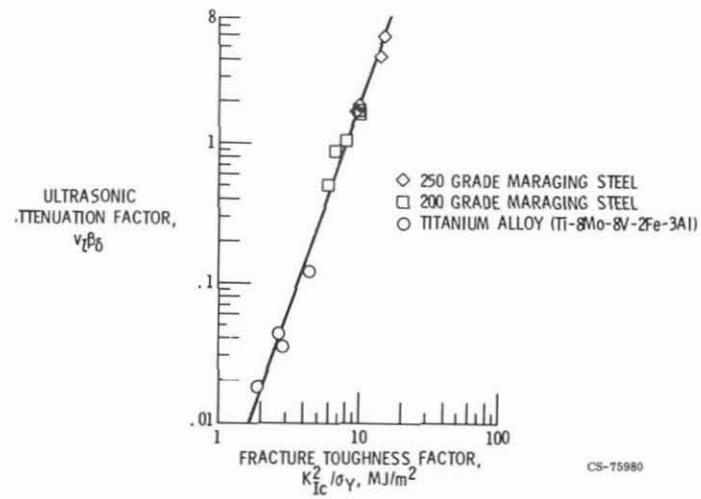

Figure 10. - Correlation of ultrasonic attenuation factor $v_l\beta_\delta$ and fracture toughness factor K_{Ic}^2/σ_Y.

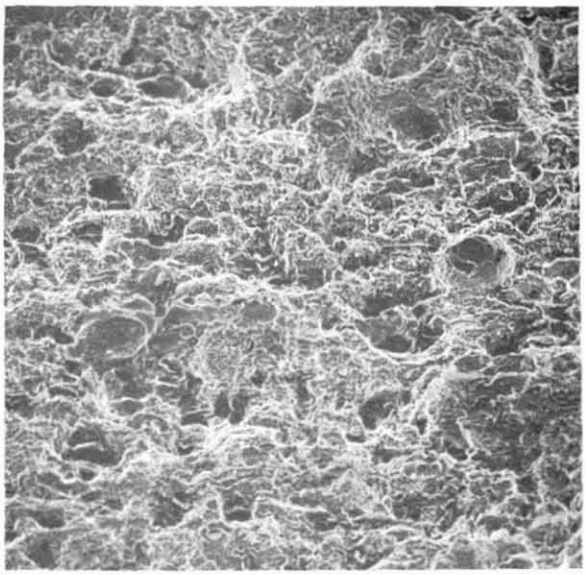

(a) FRACTOGRAPH OF 200 GRADE MARAGING STEEL, SPECIMEN 3-200, TYPICAL INDICATION OF DUCTILE FRACTURE.

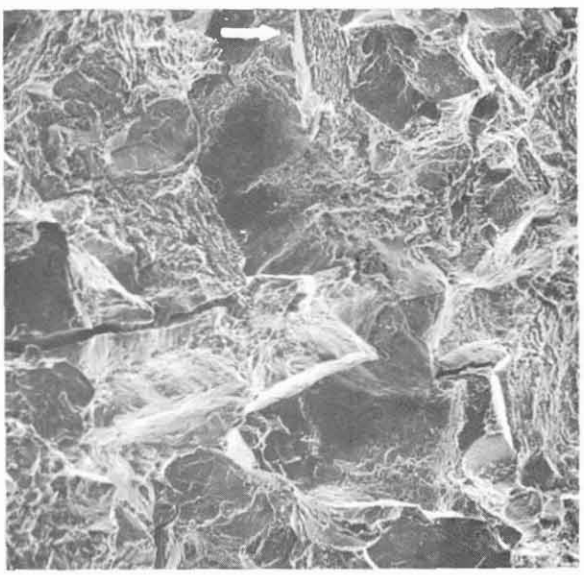

(b) FRACTOGRAPH OF TITANIUM ALLOY, SPECIMEN 3-Ti, TYPICAL INDICATION OF BRITTLE FRACTURE.

Figure 11. - Scanning electron micrographs of fracture surfaces typical of 200 grade maraging steel and titanium specimens. Original magnification was X100. Arrow indicates direction of crack extension.